J Mater Sci (2010) 45:4444–4453
DOI 10.1007/s10853-010-4527-z

A hierarchical study of the mechanical properties of gypsum

Z. Chen · S. Sucech · K. T. Faber

Received: 5 January 2010 / Accepted: 13 April 2010 / Published online: 1 May 2010

Abstract The flexural strength of gypsum is reported for freestanding single crystals in three-point bending carried with a nanoindenter. The elastic modulus, splitting tensile strength, and fracture toughness of monolithic gypsum consisting of interlocking needle-like microcrystals are also reported as functions of porosity and accelerator addition. This study shows that geometric configurations, in addition to porosity, affect the mechanical properties of gypsum. The properties are improved by 50–100% when the crystal network changes from needle aggregates to one made up of homogeneous randomly oriented single crystals. An Ashby geometric model for open-cell foams is adopted to link the properties of the individual crystals and the bulk properties. The lower and upper bounds of the measured elastic modulus are in accordance with bending-dominated behavior and stretch-dominated behavior predicted by the model, respectively. However, the strength of gypsum is much lower than values predicted by the model, which is based failure on fracture of individual crystals, suggesting that the strength of monolithic gypsum may be instead controlled by the failure of weak intercrystalline contacts.

Z. Chen · K. T. Faber (✉)
Department of Materials Science and Engineering,
Robert R. McCormick School of Engineering
and Applied Science, Northwestern University,
Evanston, IL, USA
e-mail: k-faber@northwestern.edu

S. Sucech
USG Corporation, Corporate Innovation Center, Libertyville,
IL, USA

Introduction

Gypsum is composed of an entangled network of interconnected needle-like calcium sulfate dihydrate ($CaSO_4 \cdot 2H_2O$) crystals. With porosity as high as 70% and a relatively uniform crystal size, the material can be viewed as a cellular solid, specifically an open-cell foam. Conceivably, the mechanical properties of such structures are predominantly dictated by porosity; this correlation has been extensively investigated [1]. Empirical relationships demonstrate an inverse link between the elastic modulus, hardness, flexural strength and fracture toughness of gypsum and the total porosity [2–6]. In some cases, it is desirable to lower the solid content in gypsum components for the benefit of lower cost or sound-insulation properties while retaining mechanical strength. In such instances, the improvement of mechanical properties at a given porosity is of interest, although few studies have dealt with this issue. In fact, the network structure, intercrystalline interaction, and the size of crystals and pores all affect mechanical properties of gypsum to a certain degree [7]. Amathieu and Boistelle pointed out the influence of the crystalline habits and the arrangement of crystals on the hardness of gypsum [8]. Osterwalder et al. achieved an increase in hardness by a factor of two to three by reducing the crystal size from micrometers to nanometers; the improvement was attributed to a stronger entanglement of the needle network [9]. It is believed that the mechanical properties of gypsum are affected by the properties of individual crystals as well as their arrangement. Despite these findings, the origin of the mechanical strength of gypsum remains unclear. The objective of this research is to expand our understanding of the mechanical behavior of gypsum via a hierarchical study.

The mechanical properties of individual gypsum crystals are of interest in part to develop a fundamental understanding of $CaSO_4 \cdot 2H_2O$. When the crystals form a cellular structure, although the mechanical properties of the structure as a whole could be a fraction of the properties of the crystal building blocks, they are still related to those building blocks. Thus, the properties of the crystals provide important physical input for multiscale analytical and computational models to elucidate the mechanical behavior of the bulk material. Several studies have utilized nanoindentation systems to examine the properties of solid components in porous materials [10, 11], and as load frames to examine the mechanical properties of micrometer- or nanometer-sized specimens, where compression tests [12, 13], bend tests [14], and fracture [15] have been carried out. In this study, stand-alone micron-size gypsum test specimens were prepared. Their mechanical properties were then examined, for the first time, through nanoindentation techniques. Complementing this study were tests to assess elastic modulus, strength, and fracture toughness of monolithic gypsum as a function of water-to-stucco ratio and accelerator content. Finally, models were adopted to correlate macroscopic properties with mechanical behavior of individual crystals. A hierarchical understanding of the mechanical behavior of gypsum from grains to monolithic samples was developed.

Experimental procedures

Single crystal and bulk sample preparation

Needle-like gypsum single crystals for nanoindentation tests were grown by seeded growth. Gypsum seeds were added to a supersaturated $CaSO_4$ solution prepared by mixing 0.2 M solutions of $CaCl_2$ (EMD Chemicals, Inc., Gibbstown, NY) and Na_2SO_4 (Baker Analyzed A.C.S. Reagent, Philipsburg, NJ). The seeds were prepared by collecting the precipitates produced by mixing and reaction of the same solutions. Seeding has proved to be effective in increasing the size of the crystals, but both seeded and unseeded growth yielded a combination of needle-like and twin plate morphologies. Precipitates composing mostly of large needle crystals (Fig. 1) could be produced by constantly evaporating water from the above-mentioned seeded solution at 65 °C. The crystals produced via this approach were washed and ready for mechanical testing.

The monolithic gypsum samples used in this study were prepared by hydration of a gypsum board stucco ($CaSO_4 \cdot 0.5H_2O$ (β-hemihydrate) powder produced at USG's Southard, OK plant) with and without the addition of an accelerator (ground gypsum supplied by USG). The starting powder was mixed with water (20 °C) and cast into

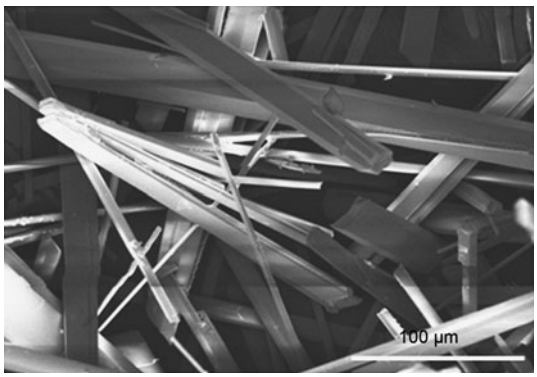

Fig. 1 Scanning electron micrograph of gypsum needle-like crystals obtained by evaporation of a seeded solution at 65 °C

split cubic (50.8 mm in length) or rectangular (150 mm × 13 mm × 9.5 mm) molds, and allowed to set. Care was taken to minimize air trapped in the paste. The setting time was approximately 30–40 min for samples without accelerator and 3 min for samples with the highest accelerator addition.

Two series of samples, each made with different water-to-stucco ratios and accelerator additions were prepared for mechanical testing. One series was prepared with no accelerator and varying water-to-stucco ratios (1, 1.5, and 2), with resultant porosities of 64%, 73%, and 78%, respectively. The porosity, p, is known to rely roughly on the water-to-stucco ratio, w, through an empirical relation, $p = (w - 0.15)/(w + 0.36)$ [16]. For the other series, the water-to-stucco ratio was kept at 1.5 while the accelerator (ground gypsum) amount was allowed to increase from 0.04 to 1.6 mg/g stucco. The accelerator addition did not change the porosity, but affected the microstructure by expediting the setting kinetics.

Microstructural characterization

Microstructure of the bulk samples was studied using a Hitachi S-4800-II cFEG scanning electron microscope (Pleasanton, CA) on fracture surfaces. To quantify the crystalline size using stereological methods, smooth surfaces were prepared by infiltrating samples with epoxy and subsequently sectioning with a microtome. The surfaces were examined in back-scattered electron mode to reveal the imbedded crystals.

Mechanical testing

Single crystals

Single crystals were used as micromechanical beams in three-point bending. Each crystal was suspended across a well created on a glass substrate. The gauge length of

the specimen was determined by the span of the well (40–50 μm). With the assistance of a micromanipulator (Custom Probes Unlimited, Terra Alta, WV), the crystals were positioned over the gap and attached to the substrate with epoxy.

A Hysitron Triboindenter (Minneapolis, MN) was used as the bend testing apparatus. This instrument can be used to apply a load of up to 10 mN and allows a maximum vertical displacement of 5 μm. In the conventional testing mode, the indenter tip is driven into the sample by applying an increasing load. The load–displacement curve is recorded continuously which can be used to extract the modulus and hardness. In this study, when used in quasi-static mode as a load frame for bend tests, most of the work goes to deflecting the material rather than indenting the material. The displacement recorded reflects the physical movement of the indenter probe even when minimum indentation of the material occurs [17].

During the test, the center of the suspended beam along its length and width was first located using an optical microscope, then confirmed by imaging in the atomic force microscope (AFM) mode. A three-sided diamond Berkovich tip was used for the loading pin. Its radius of curvature is estimated to be approximately 150 nm. Although a blunt-tipped indenter with a larger radius of curvature was deliberately used to minimize the stress concentration, the finite size of the contact point during loading is one drawback of this technique.

To deflect the sample, the indenter was operated under open-loop control to a specified maximum load with a trapezoidal load profile including 10-s loading, 5-s hold, and 10-s unloading. Each sample was loaded to fracture or until the vertical deflection limit was met. The fracture load for the specific crystal was identified from the load–displacement curve. The geometry of the crystals was determined by SEM following the test, which revealed that the cross section of the crystals was typically hexagonal, equivalent to two identical isosceles trapezoids with mirror symmetry about the central axis, where b_1 and b_2 are the length of the parallel sides of the trapezoid ($b_1 < b_2$) and d is half of the thickness of the crystal. The flexural strength of the crystals of this geometry in three-point bending is given by

$$\sigma_f = \frac{3PL}{2(3b_1 + b_2)d^2} \quad (1)$$

where P is the fracture load and L is the support span.

Bulk materials

Young's modulus of the porous gypsum bulk material was determined using a through-transmission sonic velocity method (Matec Instrument, Northborough, MA) [18, 19]. Contact transducers of 5 MHz (Technisonic, Fairfield, CT) were used for transmitting and receiving sound waves across 13 mm × 9.5 mm × 0.4 mm rectangular beams of gypsum. The longitudinal (v_l) and transverse (v_s) sonic velocities were calculated using the sample thickness and the time measured for the sonic pulse to travel through the specimen. Young's modulus E was given by

$$E = \frac{\rho v_s^2 \left(3v_l^2 - 4v_s^2\right)}{v_l^2 - v_s^2} \quad (2)$$

where ρ is the density [20].

Splitting tensile strength measurements were performed in a Sintech universal testing machine (MTS Systems Corporation, Eden Prairie, MN) using a modified Brazilian test [21]. During the test, a cube sample was loaded in compression along the face diagonal direction at a crosshead speed of 1.28 mm min^{-1}. The resultant stress distribution on the diagonal plane is tensile near the center of the diagonal at which point fracture initiates and propagates along the face diagonal plane [22].

Fracture toughness was measured using a notched-beam in four-point bending [23]. Notches with a depth-to-sample width ratio of 0.3 were introduced at the center of the rectangular samples by saw cutting, followed by insertion of razor blade to form a sharp crack. The samples were loaded at a crosshead speed of 0.005 mm min^{-1} until fracture.

Results and discussion

Single crystals

Figure 2a and c shows examples of load–deflection curves after incremental indentation to a maximum load of 500 and 3000 μN, respectively. Upon continuous loading to 500 μN, the curve appears smooth and nearly linear. On monotonic loading to 3000 μN, a series of discontinuities occur, initially at ~1400 μN, indicative of fracture initiation.

Figure 2b and d shows the corresponding AFM images of surfaces after loading to 500 and 3000 μN, respectively. No significant indentation mark is observed, while the fracture in Fig. 2d appears to be due to the cleavage of the crystal. Substituting a fracture load P of ~1400 μN and sample dimensions into Eq. 1, the flexural strength of gypsum crystals is estimated to be ~2.2 GPa. It is not unusual for micron-sized single crystals to exhibit strengths close to theoretical values. For example, the average tensile strength of SiC fibers with diameters of ~4–6 μm measured by single fiber tests was ~8.4 GPa, nearly one-fifth of its theoretical cleavage strength of 43.6 GPa [24].

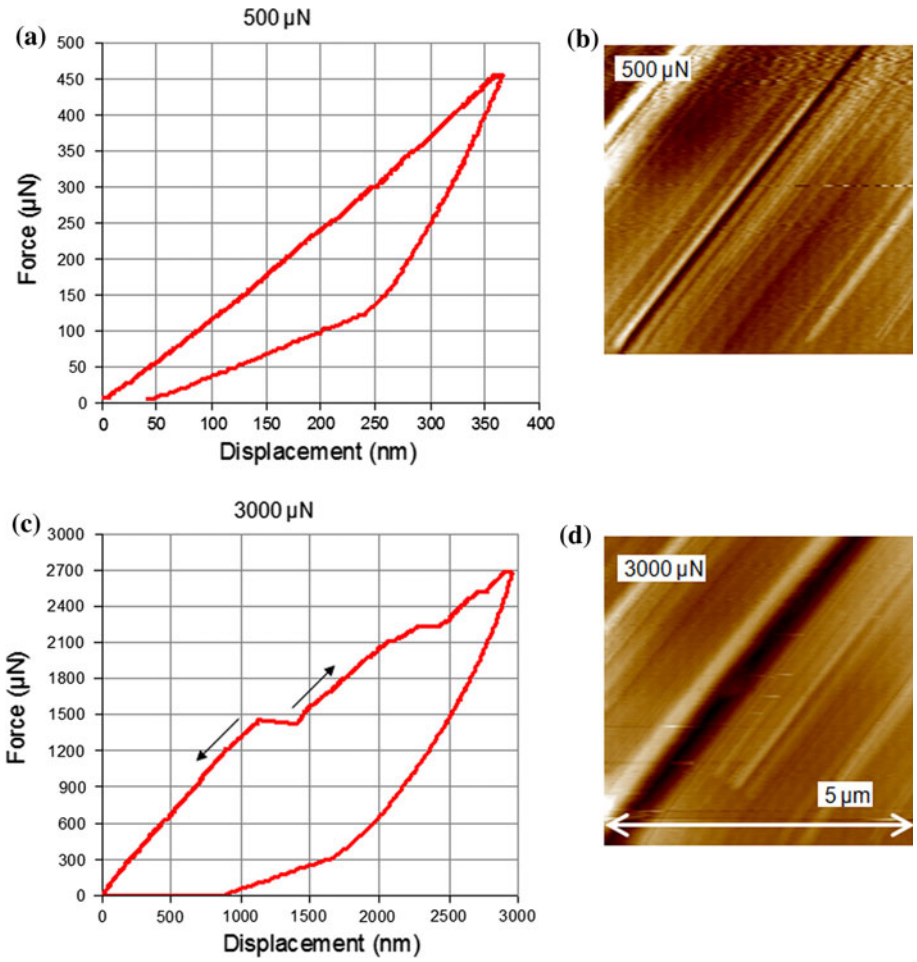

Fig. 2 **a** Force–displacement curve recorded during nanoindentation of a suspended single crystal to a maximum load of 500 µN and **b** corresponding AFM image after indentation. **c** Force–displacement curve and **d** AFM image after loading to 3000 µN. Note that the indenter was placed at the center of the image, although no indentation impressions were observed

According to X-ray diffraction, the most common extensive faces of gypsum parallelepiped crystals are those parallel to the principle cleavage planes of gypsum, namely (010), which is parallel to double sheets of the water of crystallization embedded between layers of Ca^{2+} and SO_4^{2-}. In the current experiments, the crystals possibly fractured along the (100) lattice planes, another of the easy cleavage planes of the monoclinic lattice. Figure 3 shows SEM images of crystals after fracture. A closer look at the fractured crystal reveals delamination along (010) planes parallel to the surface. The load applied during the bending test may partially separate some water sheets and crumple the $CaSO_4$ layers, causing the fracture of the crystal. Because of the discontinuous fracture path coupled with delamination, the load–deflection curve did not show a sudden drop in load, typical of catastrophic failure.

Bulk materials

The microstructure, e.g., morphology, size, and arrangement of crystals in bulk samples, is affected by the addition of accelerator. In the absence of an accelerator, needle-like crystals tend to form aggregates, or "sheaves of wheat," as shown schematically in Fig. 4a. Micrographs in Fig. 4b and c demonstrates that samples manufactured with water-to-stucco ratios of 1 and 2 are composed almost completely of aggregates. In contrast, in samples prepared with accelerators, illustrated in Fig. 4d, and pictured in Fig. 4e and f, the crystals orient more randomly, resulting a higher degree of interlocking than the aggregated sheaf-of-wheat structure.

Figure 5 shows the microstructures of samples with a water-to-stucco ratio of 1.5 with increasing accelerator amount. As the amount of the accelerator exceeds 0.2 mg/g, few aggregates are observed and the samples become a network of dispersed crystals. Despite the similar arrangement of crystals, a decrease in crystal size with higher accelerator amount is noted. Using stereological methods on microtomed sections shown in Fig. 6, and assuming the shape of an individual crystal is a square rod with end, a, and length c, where $c \gg a$, the average width of a collection of crystals can be estimated using $a = N_L/2N_A$ [25]. Here, N_L is the number of crystals per unit length and N_A is the number of crystals per unit area. The average width, a, thus measured, for samples with 0.2 and 0.8 mg/g accelerator are 2.4 and 1.7 µm, respectively. Due to

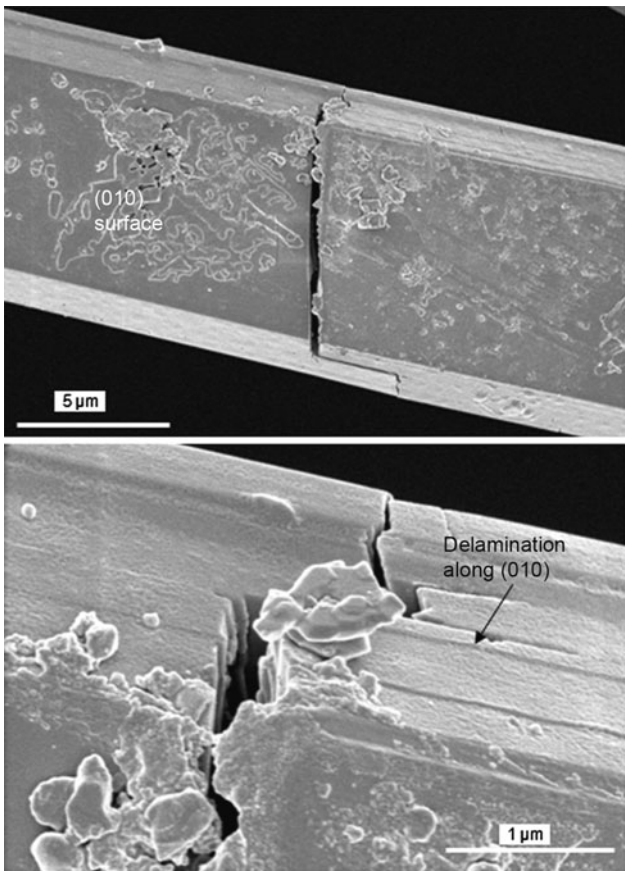

Fig. 3 SEM micrographs of gypsum single crystals after fracture

aggregation, the size of crystals in samples without accelerator is hard to quantify by the same method, although the size appears comparable to that of samples with 0.2 mg/g accelerator in Fig. 6.

Mechanical tests: the role of porosity

The correlation between mechanical properties and porosity was studied using samples with different water-to-stucco ratios. To exclude the effects of morphology, only samples without accelerator were compared. Based upon SEM micrographs, the size of the aggregates was similar among these samples; the pore size, which scales with the size of the aggregates, is also similar. Therefore, they are considered equivalent from a morphological point of view; the difference in mechanical properties is attributed solely to the change of porosity.

Young's modulus, splitting tensile strength, and fracture toughness results for samples with various water-to-stucco ratios are summarized in Fig. 7. A decreasing trend in elastic and mechanical properties with porosity is observed. Also plotted are data from Vakinis et al. [3] (circled), which cover a lower porosity range. The strength and fracture toughness decrease linearly with increased porosity in the range 45–78%. Data from Vakinis et al. appear to fall along the extrapolated trend line. A similar trend is observed for modulus.

Mechanical tests: the role of accelerators

Figure 8 summarizes the effect of accelerator on the mechanical properties of gypsum having porosities of approximately 73%. Accelerator additions as small as 0.1 mg/g stucco improve the strength, toughness, and elastic modulus. The increase of splitting tensile strength is most prominent, from 0.4 MPa, when no accelerator is added, to 0.7 MPa with 0.1 mg/g accelerator, although there is a tendency for further increase with increased accelerator. The elastic modulus increases by 60% with accelerator addition of 0.2 mg/g; further increases of the accelerator, however, do not change the modulus significantly. The fracture toughness increases by 50% with optimal amount of accelerator ($\sim$0.2–0.4 mg/g). There is a slight decrease at accelerator amounts of 0.8 mg/g; however, there is greater scatter among replicates for samples with higher accelerator amount.

The gypsum microstructure can account for some of the differences in mechanical behavior. In all cases, the greatest improvement occurs when the initial 0.1–0.2 mg/g accelerator was added to the sample, which coincides with the transition of an aggregated structure to a dispersed network of single crystals. Aggregation limits the number of contacts between neighboring crystals, as well as the interlocking arrangement of the elemental components (aggregates or single crystals). For equivalent porosities, interlocked microstructures are expected to be stiffer at a macroscopic scale, which is supported by both modeling [5] and our experimental results. A slight size variation in needle size, however, is not likely to induce significant change in the mechanical properties of gypsum.

Hierarchical relationships

Elastic properties

The elastic modulus of a foam depends on the solid of which it is made and its volume fraction or relative density, via the following equation

$$\frac{E_e}{E_s} = K\left(\frac{\rho_e}{\rho_s}\right)^n \tag{3}$$

where K and n are the constants, ρ is the density, and subscript 'e' and 's' denote the effective properties of the foam and the cell wall solid, respectively. Tuncer and Wegener summarized the characteristic exponent values for various foams where most open-cell foams demonstrated power law

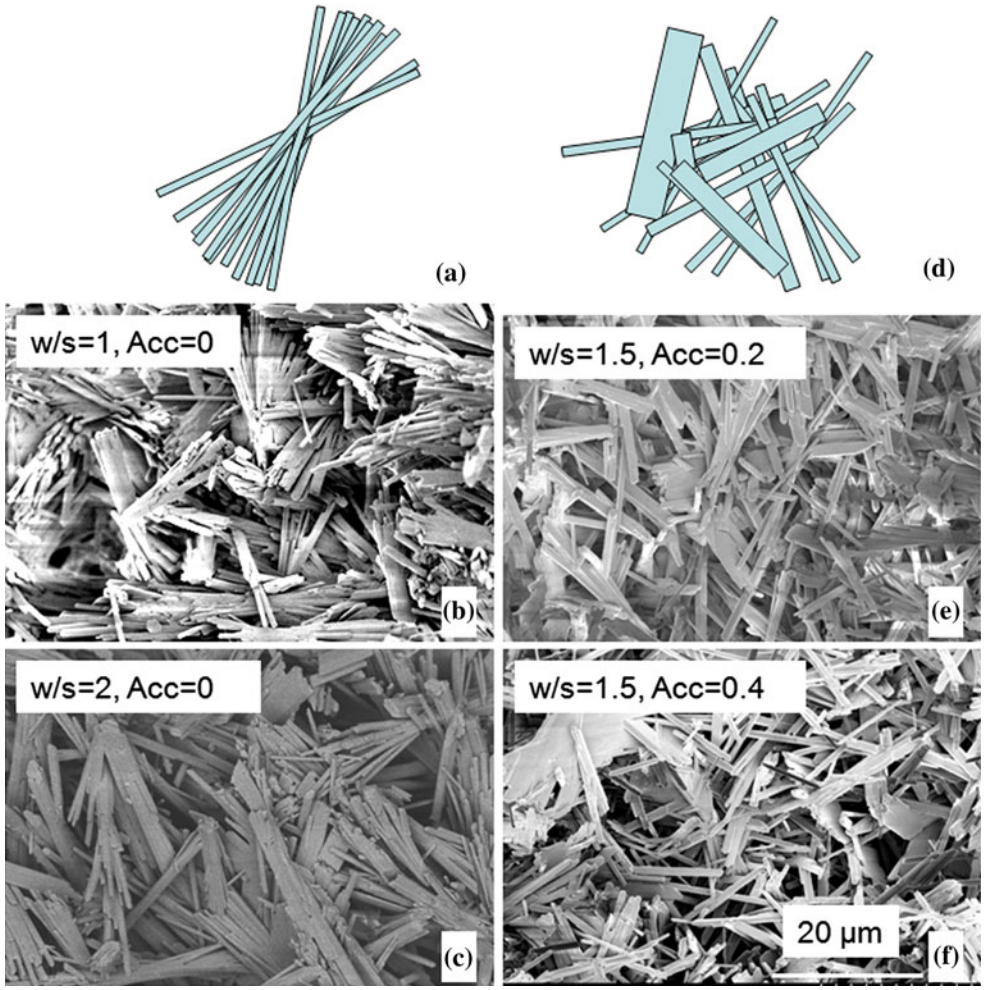

Fig. 4 Schematic and scanning electron micrographs of gypsum made with no accelerator (**a–c**) and with accelerators (**d–f**). Water-to-stucco ratio is noted by w/s; accelerator content is in units of mg/g stucco

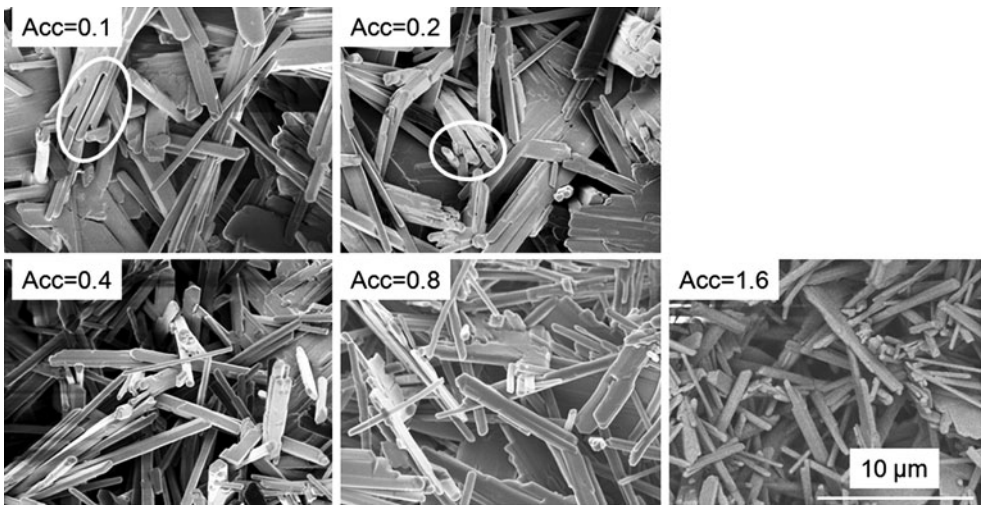

Fig. 5 Scanning electron micrographs of fracture surface as a function of accelerator content in mg/g stucco

dependence [26, 27] with $n = 2$ and the constant of proportionality K close to unity. This relation has been derived based on an idealized grid with three-dimensional translational symmetry. For dense gypsum with an elastic modulus of 25 GPa [28], the predicted elastic modulus of the gypsum with a porosity of 64–78% is in the range

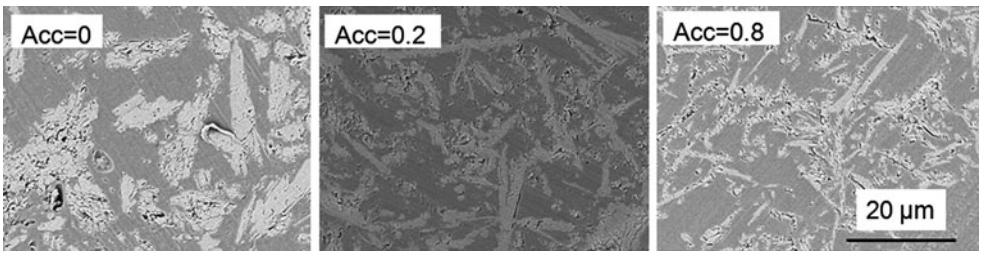

Fig. 6 Scanning electron micrographs of surfaces of monolithic gypsum prepared using a microtome. Stereological analysis confirmed a slight decrease in crystal size with increased accelerator content

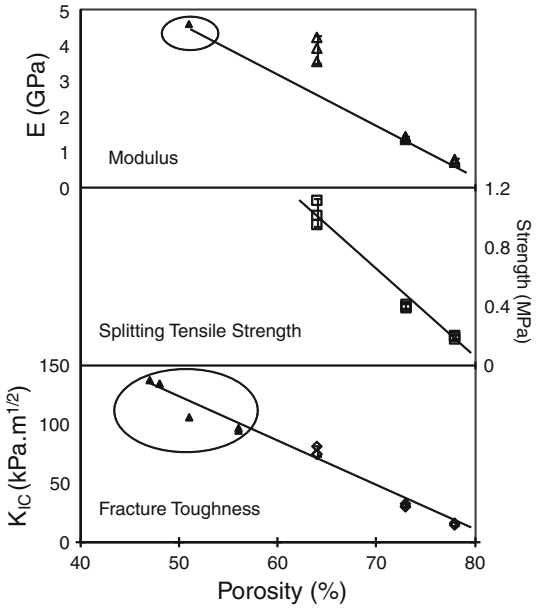

Fig. 7 Elastic modulus (*upper*), splitting tensile strength (*middle*), and fracture toughness (*lower*) as a function of porosity, which is controlled by varying water-to-stucco ratio (no accelerator added). Circled data are from Ref. [3]. Error bars indicate 95% confidence interval

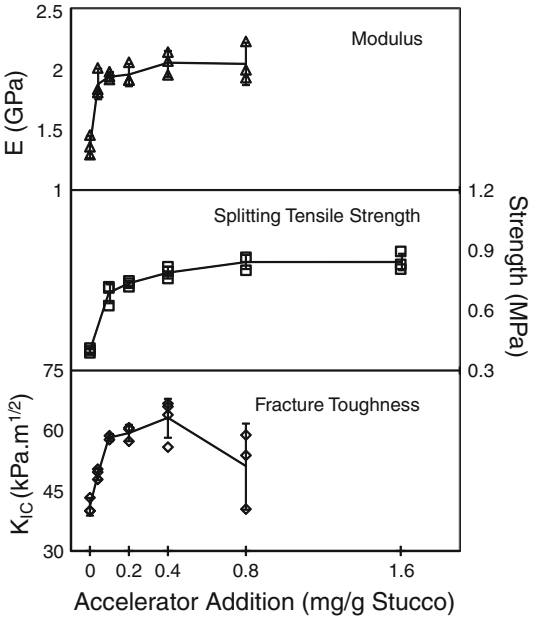

Fig. 8 Elastic modulus, splitting tensile strength, and fracture toughness as a function of accelerator addition (porosity = 73%). Error bars indicate 95% confidence interval

1.2–3.2 GPa. These agree with the values measured by the sonic velocity test.

However, this equation predicts a unique modulus at a certain relative density, and thus, cannot account for the range of moduli shown in Fig. 8 for gypsum samples of equivalent porosity but different accelerator amounts. For a relative density of 27%, the elastic modulus increases from 1.4 to 2.2 GPa when the microstructure changes from "sheaf of wheat" aggregates to a more networked structure. Apart from relative density and the intrinsic stiffness of a single needle, the configuration of the needle network also plays a role in the modulus of the open-cell structure. To explain the variation, a model by Ashby which accounts for geometric configuration is adopted. Bending- and stretch-dominated structures, which are simplified as frames composing of struts that are welded together at their joints [26], are illustrated in Fig. 9. In the bending-dominated structure (Fig. 9a), the slender struts will bend in response to external loading, whereas in the stretch-dominated structure (Fig. 9b), bending is constrained by the transverse strut. Slender structures are much stiffer when stretched in tension than when bent. While the bending-dominated configuration still exhibits the above-mentioned power law dependence on relative density (Eq. 3), for the stretch-dominated configuration, the modulus depends linearly on relative density according to

$$\frac{E_e}{E_s} = \frac{1}{3}\left(\frac{\rho_e}{\rho_s}\right) \tag{4}$$

Modulus measurements for gypsum with and without accelerator are plotted in Fig. 10 as a function of relative density along with Eqs. 3 and 4. The modulus of samples without accelerator is in good agreement with Eq. 3 when $n = 2$ and a K value of 0.8 is chosen, while those that are made with accelerators follow the stretch-dominated model, except when relative density exceeds 36%.

Our experimental results are consistent with the Ashby's lattice model relating the connectivity or crystal

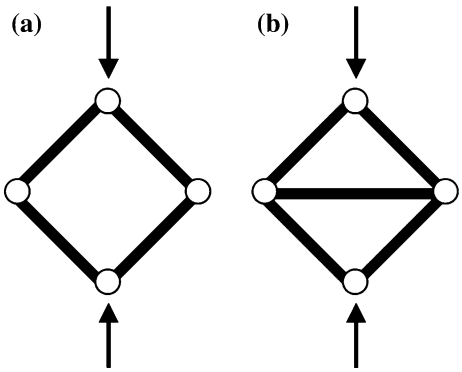

Fig. 9 **a** The pin-jointed frame for a bending-dominated structure and **b** the triangulated frame for a stretch-dominated structure

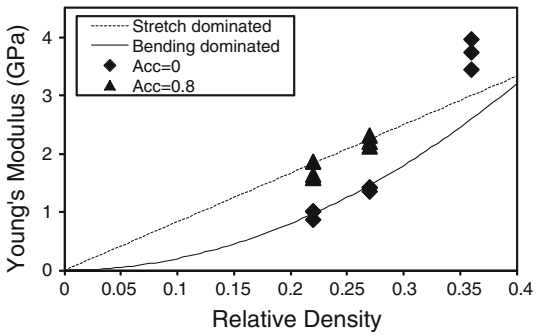

Fig. 10 The predicted elastic moduli of monolithic samples exhibit power law and linear behavior with respect to relative density (ρ/ρ_s) for bending- and the stretch-dominated deformation, respectively. The experimentally obtained moduli for samples with and without accelerators, plotted as triangles and diamonds, respectively, are consistent with the predictions

arrangement to the elastic modulus. The single crystals forming a homogeneous network apparently included the more contacts and, thus, are more constrained by their neighboring needles. Hence, it resembles a fully triangulated lattice the mechanical response of which is stretch-dominated. Conversely, if the crystals form aggregates, the number of contacts with their neighbors is reduced. The result of this lack of interlacing is that some of the crystals do not share contact points with crystals outside the aggregates. This configuration with a lower structural efficiency thus exhibits bending-dominated behavior. The modulus measured for $\rho_e/\rho_s = 36\%$, however, is higher than predicted by either configuration. We speculate that as the solid content exceeds a certain level, the interpenetration and inter-aggregate contacts become inevitable, giving rise to a higher E value.

It is noted that a high elastic modulus is only necessary when very small deflections are allowed under high load; in some cases, a gypsum component with a low elastic modulus is actually advantageous. A lower modulus can reduce stresses in a confined component which is subjected to dimensional changes caused by moisture, among other factors, and therefore lessens possible structural damage.

Fracture

Following the geometric model for strength by Ashby [26], the scaling prediction of strength assumes that the structures fail by bending- or stretch-dominated tensile fracture of the struts. The equations that correlate the macroscopic property with the property of a single strut in these two scenarios are, respectively [26],

$$\frac{\sigma}{\sigma_{f,s}} = K1\left(\frac{\rho_e}{\rho_s}\right)^{3/2} \tag{5}$$

$$\frac{\sigma_{cr}}{\sigma_{cr,s}} = K2\left(\frac{\rho_e}{\rho_s}\right) \tag{6}$$

where $\sigma_{f,s}$ and $\sigma_{cr,s}$ are flexural strength and tensile fracture strength of a strut, respectively. The constant of proportionality $K1$ is 0.2, while $K2$ is less certain and is taken as 0.2 [26]. The flexural strength of individual crystal is taken as 2.2 GPa, obtained through nanoindentation as previously described. The ratio of flexural strength to tensile strength is known to vary between 1 and 3 in brittle materials [29]. In our case, the tensile fracture strength can be roughly estimated to be the same flexural strength. The predicted strength of the cellular gypsum material is plotted in Fig. 11 for both bending and stretch fracture. The prediction of strength of the bulk material with a porosity of 73% based on the failure modes are approximately 60 and 120 MPa, respectively. In contrast, the experimental values (plotted in the inset of Fig. 11) are 0.4–0.9 MPa, two orders of magnitude lower than the prediction.

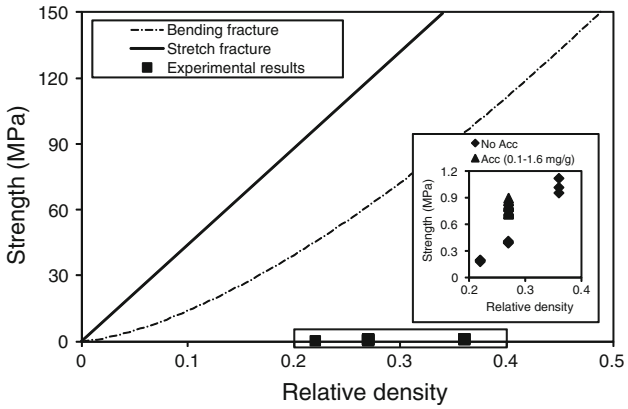

Fig. 11 Predicted strength of monolithic gypsum samples when the fracture is dominated by bending (*dotted line*) or tensile fracture (*solid line*) of a strut. Also plotted are strength values obtained experimentally. These values are re-plotted using an expanded scale in the *inset*

Strength prediction based on geometric configuration and single crystal properties is not an accurate predictor of strength, unlike elastic modulus. The magnitude of the discrepancy is likely due to incorrect assumptions rather than due to the inadequacies of the model. Both bending and stretch fracture models assume that failure initiates from individual struts, while the joints are considered to be plastic hinges or unbreakable pins. By taking the bulk strength of 0.4–0.9 MPa, the flexural and tensile strength of an individual crystal was estimated by reverse analysis of Eqs. 5 and 6 to be 14 and 17 MPa, respectively. This derived strength is the failure strength of the weakest link in the solid skeleton, and far below the stress at which the crystals reach their elastic limit from single crystal experiment ($\sim$2 GPa). More likely the value of 14–17 MPa is indicative of the strength of the intercrystalline contact. Contrary to the model assumption, the joints between crystals are not unbreakable; bearing high stress, they fail before the fracture of individual crystals. Their strength in gypsum bulk material has never been measured directly, but an analog can be drawn from mica, in experiments in which two atomically smooth surfaces were brought in contact and the shear force between them measured. According to the available data in the literature for mica, the shear stress between two surfaces in contact is $\sim$60 MPa [30]. A previous study by Satava [16] also found that the strength of gypsum is proportional to the contact area. Through the experiment, the author demonstrated that mechanical failure occurs at the contact, which corresponds to the point with a weak bond.

The nature of such intercrystalline bonding is still under debate. Some suggest that the cross-like intergrowth of needles are due to twinning, and therefore, the bonding is ionic–covalent at the boundaries [31] and some believe that a cement-like phase is deposited between gypsum needles by the solution during the last stages of setting and acts as glue to bond the crystals together [32]. Yet, another model, the bonding water model, suggests that the adjacent crystals are joined through a thin layer of water [33]. According to this model, van der Waals forces and double-layer interactions are crucial for the bonding between micron-size gypsum needles because of the parallelism of needles in contact that affords large contact area. The interactions at very small distance of separation (<2 nm), which are probably equivalent to the oscillatory forces measured between mica surfaces by Israelachvili and Pashley [34], give rise to adhesion between two crystals. Since periodicity of the oscillations measured in their experiment is about 0.25 nm, roughly corresponding to the diameter of the water molecule, it has been proposed that the water molecules assume a regular packing arrangement when trapped between surfaces of this small separation. According to our experimental data and in comparison with the Ashby model, a relatively weak bonding strength is expected; therefore, bonding originating from ionic–covalent interactions of solid which gives rise to high interfacial strength is unlikely. Strengths of this magnitude are more likely due to the hydrogen bonding proposed in bonding water model.

Conclusions

The elastic and mechanical properties of gypsum at high porosities are investigated. Our study has indicated that the mechanical properties are not only a function of porosity, but also are dependent upon the arrangement of crystals in the bulk sample as well as intercrystalline bonding strength. A homogeneous microstructure of randomly oriented single crystals, which gives rise to a stretch-dominated behavior, demonstrates higher elastic and mechanical properties than the alternative bending-dominated structure which consists of "sheaf of wheat" aggregates. In the elastic regime, the elastic modulus benefits from the increased connectivity induced by this stretch-dominated structure and increases by 60% compared to the alternative bending-dominated configuration. The splitting tensile strength can be improved by as much as 100% over that of the bending-dominated structure due to the increased number of contacts. However, the strength of the individual crystals is not a determining factor to the strength of gypsum. In contrast to Ashby's lattice model of connectivity, gypsum fails under a load far below that which causes the fracture of individual crystals. It is, therefore, more likely that fracture initiates at the sites of intercrystalline bonding.

Acknowledgements Support for this study was provided by USG Corporation. The nanoindentation work was performed at the NIFTI facilities of NUANCE Center at Northwestern University. The SEM work was performed at the EPIC facilities of NUANCE Center. NUANCE Center is supported by NSF-NSEC, NSF-MRSEC, Keck Foundation, the State of Illinois, and Northwestern University.

References

1. Gibson LJ, Ashby MF (1997) Cellular solids, structure and properties, 2nd edn. Cambridge University Press, Cambridge, UK
2. Soroka I, Sereda PJ (1968) J Am Ceram Soc 51(6):337
3. Vekinis G, Ashby MF, Beaumont PWR (1993) J Mater Sci 28:3221. doi:10.1007/BF00354239
4. Sattler H (1997) ZKG Int 50(1):54
5. Meille S, Garboczi EJ (2001) Modell Simul Mater Sci Eng 9:371
6. Jeulin D, Monnaie P, Peronnet F (2001) Cem Concr Compos 23:299
7. Singh NB, Middendorf B (2007) Prog Cryst Growth Char Mater 53(1):57
8. Amathieu L, Boistelle R (1986) J Cryst Growth 79(1–3):169

9. Osterwalder N, Loher S, Grass RN, Brunner TJ, Limbach LK, Halim SC, Stark WJ (2007) J Nanopart Res 9:275
10. Constantinides G, Ulm F-J (2004) Cem Concr Res 34:67
11. Kaul VS, Faber KT (2008) Scr Mater 58:886
12. Uchic MD, Dimiduk DM, Florando JN, Nix WD (2004) Science 305(5686):986
13. Schuster BE, Wei Q, Zhang H, Ramesh KT (2006) Appl Phys Lett 88(10):103112
14. Lee D, Wei XD, Zhao M, Chen X, Jun SC, Hone J, Kysar JW (2007) Modell Simul Mater Sci Eng 15:S181
15. Chen X, Xu Z, Li X, Shaibat MA, Ishii Y, Ruoff RS (2007) Carbon 45(2):416
16. Satava V (1996) Ceramics-Silikaty 40(2):72
17. Oliver WC GM, Pharr GM (2004) J Mater Res 19:3
18. ASTM Standard C769-98 (2005) Standard test method for sonic velocity in manufactured carbon and graphite materials for use in obtaining an approximate Young's modulus
19. ASTM Standard C1419-99a (2007) Standard test method for sonic velocity in refractory materials at room temperature and its use in obtaining an approximate Young's modulus
20. ASTM Standard E494-05 (2005) Standard practice for measuring ultrasonic velocity in materials
21. Miller DP, Moslemi AA (1991) Wood Fiber Sci 23(4):472
22. Jonsén P, Häggblad H-Å, Sommer K (2006) Tensile strength and fracture energy of pressed metal powder by diametral compression test. Doctoral thesis, D1-D18
23. ASTM C 1421-01b (2001) Standard test methods for determination of fracture toughness of advanced ceramics at ambient temperature
24. Petrovic JJ, Milewski JV, Rohr DL, Gac FD (1985) J Mater Sci 20:1167. doi:10.1007/BF01026310
25. Underwood EE (1970) Quantitative stereology. Addison-Wesley, Publishing Co., Inc., Reading, MA
26. Ashby MF (2006) Phil Trans R Soc A 364:15
27. Tuncer E, Wegener M (2004) Mater Lett 58:2815
28. Broz ME, Cook RF, Whitney DL (2006) Am Mineral 91:135
29. Maalej M, Li VC (1994) J Mater Civ Eng 6(4):513
30. Ohnishi S, Stewart AM (2002) Langmuir 18:6140
31. Follner S, Wolter A, Helming K, Silber C, Bartels H, Follner H (2003) Cryst Res Technol 37(2–3):207
32. Coquard P, Boistelle R (1994) Int J Rock Mech Min Sci Geomech Ahslr 31(5):517
33. Chappuis J (1999) Colloids Surf A Physicochem Eng Asp 156:223
34. Israelachvili JN, Pashley RM (1983) Nature 17:249